Archives of Acoustics Vol. **47**, No. 3, pp. 373–382 (2022), doi: 10.24425/aoa.2022.142011

Research Paper

Ultrasonic Simulation Research of Two-Dimensional Distribution in Gas-Solid Two-Phase Flow by Backscattering Method

Jinhui FAN, Fei WANG*

State Key Laboratory of Clean Energy Utilization, Zhejiang University
Hangzhou, 310027, China

*Corresponding Author e-mail: wangfei@zju.edu.cn

(*received November 11, 2021; accepted April 27, 2022*)

The two-dimensional distribution of gas-solid flow parameters is a great research significance to reflect the actual situation in industry. The commonly used method is the ultrasonic tomography method, in which multiple probes are arranged at various angles, or the measurement device is rotated as that in medicine, but in most industrial situations, it is impossible to install probes at all angles or rotate the measured pipe. The backscattering method, however, uses only one transducer to both transmit and receive signals, and the two-dimensional information is obtained by only rotating the transducer. Ultrasound attenuates greatly in the air, and the attenuation changes with frequency. Therefore, COMSOL is used to study the reflection of particles with different radii in the air to ultrasound with various frequencies. It is found that the backscattering equivalent voltage is the largest when the product of ultrasonic frequency and particle radius is about 27.78 Hz · m, and the particle concentration of 30% causes the strongest backscattering. The simulated results are in good agreement with the Faran backscattering model, which can provide references for selecting the appropriate frequency and obtaining the concentration when measuring gas-solid two-phase flow with the ultrasonic backscattering method.

Keywords: gas-solid two-phase flow; COMSOL simulation; ultrasonic backscattering method.

1. Introduction

Gas-solid two-phase flow occurs widely in industry, such as pneumatic conveying of solid particles, and pulverized coal-air two-phase flow in the circulating fluidized bed, etc. In these industrial processes, the parameters to be measured are mainly the concentration and radius of solid particles, and it is important to realize the real-time measurement of them in the gas-solid two-phase flow. For example, for the circulating fluidized bed, the real-time measurement and timely adjustment of the particle radius and concentration of pulverized coal are meaningful for improving combustion efficiency, preventing choking and other safety problems, and for reducing pollutant discharge and energy consumption (Jing *et al.*, 2011). For the measurement of particle concentration and radius in the gas-solid two-phase flow, researchers have proposed many methods, such as the differential pressure method (Shaffer, Bajura, 1990), optical methods (Wang *et al.*, 2018; Cai *et al.*, 2005), and electrical methods etc., but all of these methods have their own shortcomings. The principle of the differential pressure method is pressure difference, but the results are accurate only when the concentration is high (Han *et al.*, 2016). The instruments used in optical methods are generally more precise, expensive, and sensitive to field conditions (Sakamoto, Saito, 2012; Ma *et al.*, 2021). The electrical method requires the measured medium to have certain electrical properties, so its application scope is limited (Meng *et al.*, 2010). With the advantages such as strong penetration, not being affected by concentration, no interference to the flow field, and its capacity for continuous on-line measurement, acoustic methods have attracted extensive attention from researchers and have been applied to two-phase flow measurement (Awad *et al.*, 2012; Boonkhao, Wang, 2012; Gu *et al.*, 2018). There are many ultrasonic measurement methods, but in most cases, the ultrasonic attenuation method is selected for measuring two-phase flow (Dong *et al.*, 2020; Tsuji *et al.*, 2019). Specifically, the signal detected by two transducers placed at opposite ends of the pipe is used to reflect the concentration and radius change of particles in gas-solid two-phase flow (Tian *et al.*, 2013; Chen *et al.*, 2020).

The ultrasonic attenuation method is effective when using for one-dimensional measurement, but it still faces many challenges when applied to two-dimensional measurement. For example, it requires multiple transmitting and receiving transducers to form multiple measuring circuits (ultrasonic process tomography) (Yao, Takei, 2017), in which transducers are needed to be placed 360° around the pipe (as shown in Fig. 1a), or it can be achieved by rotating the system, which is impossible in most industrial applications, and may cause safety risks in production. Thus, to put forward a new method of gas-solid two-phase flow measurement is of great significance.

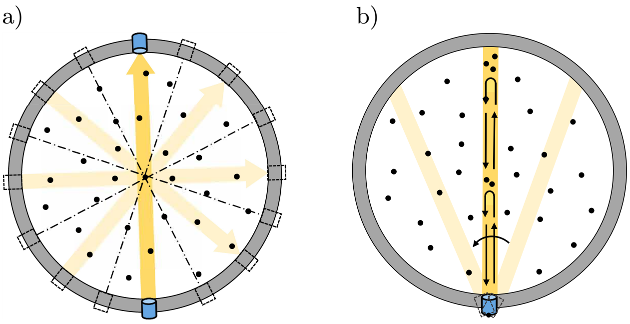

Fig. 1. Arrangement of transducers in the two measurement methods: a) the ultrasonic attenuation method, b) the ultrasonic backscattering method.

Different from the transmission principle of the ultrasonic attenuation method, the backscattering mode may be the effective technical approach, in which the transmission and reception of ultrasound are completed by the same transducer in one-dimensional measurement (Mathieu, Schweitzer, 2004; Dukhin *et al.*, 2000). The two-dimensional measurement can be achieved by only rotating the transducer across the cross-section, which is more practical in industrial measurement (as shown in Fig. 1b). This method is similar to reflection, but the difference is that reflection generally refers to the interaction of ultrasound with particles much larger than the wavelength of the ultrasound, whereas when particles are much smaller than the wavelength of the ultrasound, the interaction is called scattering (Anderson, 1950). The backscattering (the scattering angle is around 180°) method is based on the interaction between the signal and the target in the gas, especially the scattering characteristic. During the backscattering measurements, after ultrasonic transducer transmits the pulse wave, the parameters can be determined quantitatively or semi-quantitatively according to the intensity of echo signal reflected by particles. Compared with the ultrasonic process tomography method, the backscattering method does not require installing detectors at all degrees, which greatly simplifies the measurement system and makes the operating procedures more convenient (Jia *et al.*, 2017).

The ultrasonic backscattering method has been used in some industrial fields. Weser *et al.* (2013; 2014) proposed a semi-empirical method to measure particle radius and concentration in liquid-solid two-phase flow, the equivalent sound attenuation and scattering amplitude are obtained after the statistical analysis of the scattered signals of particles, then the radius and concentration can be known. Elvira *et al.* (2016) also used the backscattering method with high-frequency ultrasound to measure the concentration of yeast suspensions, which proved the effective application of the ultrasonic backscattering method in micron particle measurement. Furlan *et al.* (2012) measured the concentration of sodium-calcium glass particles (195 μm in diameter) in the slurry by backscattering method, and achieved accurate results (Furlan *et al.*, 2012). But these applications are all liquid-solid two-phase flows, in the field of gas-solid two-phase flow, the employment of ultrasonic backscattering method still faces many challenges. For example, the attenuation of ultrasonic waves in the air is much faster than that in the liquid or solid; the higher the ultrasonic frequency is, the larger the attenuation will be (as shown in Table 1); the reflection echo of smaller particles is too weak, and so on (Epstein, Carhart, 1953).

Table 1. Propagation distance [km] when ultrasound attenuates to 1/e.

Frequency [kHz]	Air	Water
20	$1.89 \cdot 10^{-1}$	$3.13 \cdot 10^{2}$
50	$3.03 \cdot 10^{-2}$	$5.01 \cdot 10$
100	$7.58 \cdot 10^{-3}$	$1.25 \cdot 10$
1000	$7.58 \cdot 10^{-5}$	$1.25 \cdot 10^{-1}$

In this paper, we demonstrate the feasibility and influencing factors of ultrasonic backscattering method in gas-solid two-phase flow by simulating the reflection intensities of different radii and concentrations of particles in the air to ultrasonic waves with different frequencies. The research is based on the finite element analysis software COMSOL, and the simulation results are verified by the Faran model. The results show that the backscattering intensity is the largest when the product of ultrasonic frequency and particle radius is about 27.78 Hz · m, and the particle concentration of 30% causes the strongest backscattering. This work can provide the theoretical basis for the selection of ultrasonic frequency and the determination of particle size and concentration information in actual measurement, and also a solution for the novel measurement method for two-dimensional distribution in gas-solid two-phase flow.

The paper is structured as follows. The theoretical background of backscattering method and the Faran model is introduced in Sec. 2. In Sec. 3 the simulation model, modelling basis, simulation process, corresponding results, and verifications of results are developed. The results are discussed in Sec. 4. Finally, Sec. 5 summarizes the main conclusions.

2. Theory of backscattering method

When the ultrasonic wave is incident on isotropic particles, it scatters in all directions. Depending on different scattering angles, the scattered wave can be divided into forward scattering, lateral scattering, and backward scattering, as shown in Fig. 2a. It is forward scattering when the scattering angle is less than 90°, and if the scattering angle is between 90° and 180°, it is backward scattering (backscattering); otherwise, it is lateral scattering (Anderson, 1950). The schematic diagram of backscattering is shown in Fig. 2b.

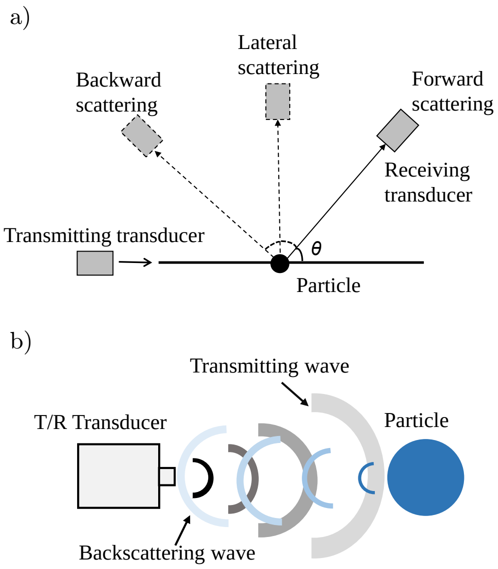

Fig. 2. Schematic diagram of three kinds of ultrasonic scattering mechanisms and details of backscattering: a) three kinds of scattering, b) diagram of backscattering.

Faran first studied the scattering that the ultrasound incidents to the cylinder or sphere, and put forward the complete single-particle scattering model, which was in good agreement with the experimental results. In Faran's opinion, solid particles can be regarded as the rigidly fixed ball when the grain density is greater than that of fluid, and the expression of single-particle scattering sound pressure as follow (Faran Jr., 1951):

$$P = \widehat{P}_0 \frac{ie^{ikr}}{kr} \sum_{n=0}^{\infty} (2n+1) P_n(\cos\theta) A_n, \tag{1}$$

$$A_n = -\sin\eta_n \cdot e^{-i\eta_n} = \frac{-i \cdot \tan\eta_n}{1 + i \cdot \tan\eta_n}, \tag{2}$$

where

$$\tan\eta_n = \tan\delta_n(ka) \frac{\tan\alpha_n(ka) + \tan\Phi_n(k_L a, k_T a)}{\tan\beta_n(ka) + \tan\Phi_n(k_L a, k_T a)}, \tag{3}$$

and

$$\tan\delta_n(ka) = -\frac{j_n(ka)}{n_n(ka)}, \tag{4}$$

$$\tan\alpha_n(ka) = -\frac{ka \cdot j_n'(ka)}{j_n(ka)}, \tag{5}$$

$$\tan\beta_n(ka) = -\frac{ka \cdot n_n'(ka)}{n_n(ka)}. \tag{6}$$

$$\tan\Phi_n(k_L a, k_T a) = \frac{\rho_c (k_T a)^2}{2\rho_d} \cdot \left[\frac{\dfrac{X^*}{X^*+1} - \dfrac{n^2+n}{n^2+n-1-\frac{(k_T a)^2}{2}+Y^*}}{\dfrac{n^2+n-\frac{(k_T a)^2}{2}+2X^*}{X^*+1} - \dfrac{(n^2+n)(Y^*+1)}{n^2+n-1-\frac{(k_T a)^2}{2}+Y^*}} \right], \tag{7}$$

where

$$X^* = \tan\alpha_n(k_L a),$$

$$Y^* = \tan\alpha_n(k_T a).$$

Dimensionless wavenumber ka:

$$ka = \frac{2\pi}{\lambda} \cdot \frac{x}{2} = \frac{\pi \cdot x}{\lambda} = \frac{\pi \cdot f \cdot x}{c}, \tag{8}$$

where x refers to particle radius, f is the sound frequency, λ is the wavelength, c is the sound velocity, k is the wavenumber, a is the particle radius, the derivatives of Bessel function and Neumann function (j_n', n_n') represent the differentiation relative to dimensionless wavenumber ka, and the angular distribution of scattering amplitude of the scattering wave is represented by the Legendre polynomial P_n of the n-th order (Hwang, Chen, 2007):

$$P_0(\cos\theta) = 1,$$

$$P_n(\cos\theta) = \frac{1}{2^n n!} \frac{d^n}{d(\cos\theta)^n} \left| (\cos^2\theta - 1)^n \right|, \qquad n = 1, 2, ... \tag{9}$$

The dimensionless wavenumber of a longitudinal wave inside the particle:

$$k_L a = \frac{\pi x f}{c_{d.L}}. \tag{10}$$

The dimensionless wavenumber of a compressional wave inside the particle:

$$k_T a = \frac{\pi x f}{c_{d.T}}. \tag{11}$$

The Faran model can be applied to flow with solid particles or fluid particles, for it takes into account the propagation of longitudinal and compressional waves inside particles and is not affected by particle radius. Therefore, the Faran model is selected for theoretical analysis in this paper (Weser *et al.*, 2013).

Assuming that the number of particle phases is N and each particle is considered to be incoherent, the total scattered sound pressure is:

$$P_{\Sigma} = P \cdot N = P \cdot \frac{c_V}{V_P}, \tag{12}$$

where V_P represents the volume of a single particle, and c_V is the volume concentration of N particles dispersed in the surrounding medium. When many particles exist at the same time, they may interact with each other. To study the backscattering intensity in this situation (Twerskyt, 1975), Percus and Yevick (1958) proposed the concept of the packing factor W, which is the degree of free space among particles. It decreases with the increase in particle concentration. The expression of the packing factor related to concentration is given as:

$$W(c_V) = \frac{(1 - c_V)^4}{(1 + 2c_V)^2}. \tag{13}$$

By substituting it into Eq. (12), the total backscattered sound pressure at a certain concentration can be obtained:

$$P_{\Sigma} = P \cdot \frac{c_V}{V_P} \cdot W(c_V) = \frac{P}{V_P} \cdot c_V \cdot W(c_V). \tag{14}$$

3. Simulation model

3.1. Introduction of simulation modelling

COMSOL is a multi-physical field simulation software, which can realize the design and optimization of practical engineering problems by simulating physical phenomena in real scenes. All the steps involved in the modelling workflow can be implemented in COMSOL, from geometric modelling, defining material properties, setting up physical fields for describing physical phenomena, solving the model, as well as post-processing the model to provide accurate and credible results. Therefore, COMSOL software is chosen to simulate the backscattering of particles in the gas-solid two-phase flow (Khushrushahi, Zahn, 2011).

In the actual field, taking pulverized coal transmission pipeline as an example, the concentration and particle size distribution on the two-dimensional circular cross section is mainly concerned, rather than the changes in the three-dimensional pipe, so the two-dimensional model is chosen for simulation. Besides, the two-dimensional model can greatly reduce the calculation time and improve the efficiency of simulation (Wang *et al.*, 2016). In the simulation, the solid particles with different radii were placed in the center of the measured pipeline, which is full of gas, and the simulation model structure is shown in Fig. 3. The pipe diameter R is 150 mm, and the diameter and thickness of the ultrasonic transducer are 10 mm and 5 mm, respectively. The main concern is the propagation of sound rather than the structure of the transducer in the simulation process, so the piezoelectric material PZT-5H is briefly considered as the transducer, the continuous phase medium and the discrete phase particles are self-added materials, and the relevant parameters are shown in Table 2.

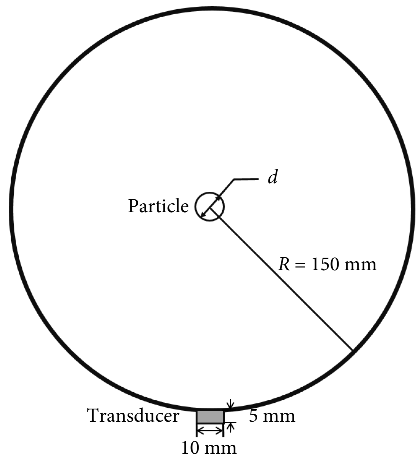

Fig. 3. Simulation model structure of a circular pipe and a particle.

Table 2. Physical parameters of air and particles.

Physical properties	Air	Particle	PZT-5H
Density [kg/m^3]	1.225	2250.0	7500
Longitudinal wave velocity of sound [m/s]	339.9	2500.0	4560
Shear wave velocity of sound [m/s]	–	1366.9	2375

Meshing is an important process for simulation, which will directly affect the calculation accuracy. The maximum element of this simulation was selected as 1/7 of the wavelength (Wang *et al.*, 2017). The pipeline, ultrasonic transducer and solid particles were treated with relatively extremely refined, and extremely refined, respectively. Figure 4 shows the simulation model after grid processing, in which the transducer and solid particles are mapped, and the pipeline is divided into the form of the free triangular grid. The distance of ultrasonic reflected to the farthest pipe wall is twice the diameter of the pipe, and the transmission speed of ultrasonic in the air is about 340 m/s. Therefore, in order to make obtained data complete, the solution time should be no less than:

$$t = \frac{2d}{v} = \frac{2 \cdot 300\ \text{mm}}{340\ \text{m/s}} = 1.76\ \text{ms}. \tag{15}$$

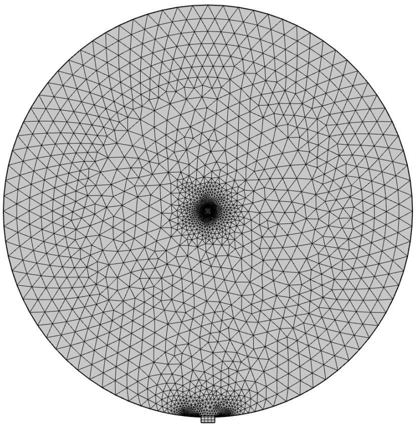

Fig. 4. Simulation model with grid processing.

Finally, the solution time was set to 2 ms, and the actual simulation time was about 8 minutes.

3.2. The coupling equation of electricity-structure-sound system

The piezoelectric material (the transducer) can produce ultrasonic waves when excited by the Gaussian pulse with an amplitude of 220 V (as shown in Fig. 5). Gaussian pulse is selected because the main lobe of Gaussian pulse is wider and the side lobe suppression is better compared with other pulses. The terminal type is set to a circuit, which is shown in Fig. 6 to make the transducer used for both transmitting and receiving ultrasonic waves. Node 0 is set as grounding, node 0 to 1 is a 220 V voltage source, from node 1 to 2

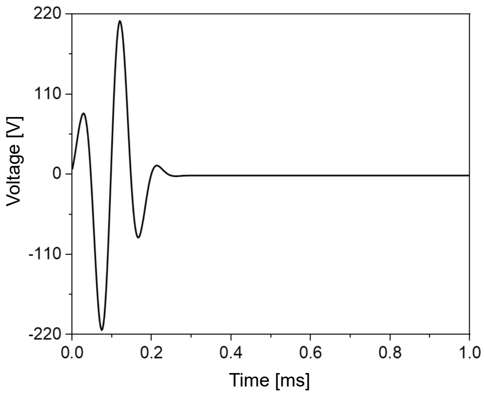

Fig. 5. Waveform of Gaussian sinusoidal pulse.

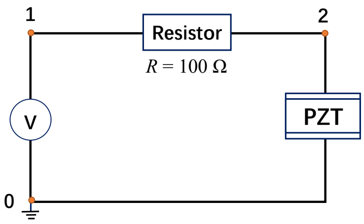

Fig. 6. Equivalent circuit diagram of the terminal.

of the circuit a resistance with 100 Ohm is placed to ensure the safety of the circuit, and node 2 to 0 is piezoelectric ceramics. When the ultrasonic wave propagates in the air, it encounters particles and is reflected by the particles. The reflected ultrasonic signals are converted into electrical signals by the data acquisition process, and are transmitted to the computer. The finite element analysis of this process mainly involves the coupling of three physical fields: electricity-structure-sound, in which the wave equation of the sound field is:

$$\frac{1}{\rho c^2}\frac{\partial^2 p}{\partial^2 t} + \nabla \cdot \left(-\frac{1}{\rho c}(\nabla p t)\right) = 0, \tag{16}$$

where ρ is the material density, c is sound velocity, P refers to sound pressure, ∇ is Laplace operator, t is time.

The equation of the structural mechanic is:

$$\rho\frac{\partial^2 u}{\partial^2 t} = \nabla \cdot s + F_V, \tag{17}$$

where u is the displacement, s is the stress, and F_V is the volume force.

Maxwell's equation of the electric field is:

$$\nabla \cdot D = \rho_V, \tag{18}$$

where D is the electrical displacement and ρ_V is the volume charge density (Louisnard, 2012).

In the simulation, the pipe wall is set as the hard sound field boundary, the inner boundary of the ultrasonic transducer is set for the transmitting-receiving end, and the acoustic boundary condition is sound-structure coupling. The outer boundary condition of the ultrasonic transducer is ground, and roller support is chosen for the structure boundary condition to prevent unnecessary movement caused by sound propagation.

3.3. Simulation process and analysis

3.3.1. The effect of particle radius on backscattering at different frequencies

The particle radius r was set from small to large to be 0.2 mm, 0.3 mm, 0.4 mm, 0.6 mm, and 1.0 mm, and the frequencies were 30 kHz, 50 kHz, 75 kHz, 100 kHz, and 150 kHz, respectively to study the backscattering of the particle with different radii to ultrasonic signals with different frequencies. The ultrasonic wave emitted by the transducer will be reflected by particles and the echo will be received by the transducer. Figure 7 shows the backscattering waveform of particles when the frequency is 100 kHz and the radius is 0.3 mm. The frequency domain signal (equivalent voltage varies with frequency) obtained by Fast Fourier Transformation of backscattered time-domain signal (equivalent voltage versus time) is shown in Fig. 8.

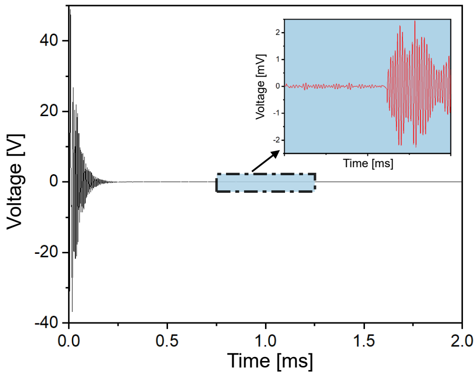

Fig. 7. The backscattering waveform of particles when the frequency is 100 kHz and the radius is 0.3 mm.

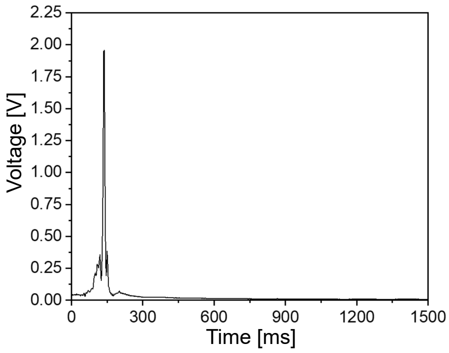

Fig. 8. The frequency-domain signal obtained by FFT.

The simulated reflected amplitude of particles with different particle radii at different frequencies is shown in Fig. 9. It can be seen that the backscattering equivalent voltage is much larger when the frequency changes from 75 to 150 kHz than that when frequencies are 30 and 50 kHz; the backscattering is not getting stronger with the higher frequency, but presents the maximum value at 100 kHz; and the higher the frequency is, the smaller the particle radius corresponding to the maximum equivalent voltage is.

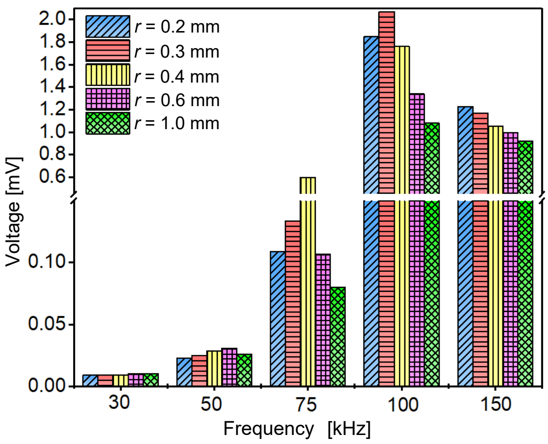

Fig. 9. Relation diagram of backscattering equivalent voltage with the variation of frequency and particle radius.

3.3.2. Verification of the effect of particle radius on backscattering at different frequencies

The Faran model was researched to describe the relationship between the equivalent voltage amplitude of particle backscattering, frequency and particle radius. The parameters of the continuous phase and dispersed phase used are the same as shown in Table 2. According to Eq. (1) to Eq. (7), when the dispersed phase and the continuous phase are determined, namely, after the related parameters of both phases are known, the dimensionless wavenumber ka is the only parameter affecting the backscattering sound pressure. Therefore, the relationship between the backscattering sound pressure and the dimensionless wavenumber ka can be studied in theory to validate the simulation results.

Figure 10 shows how relative backscattering amplitude (the backscattering voltage divided by the emission voltage, normalized) changes with dimensionless wavenumber when the scattering angle is 180°. It can be seen that when other conditions are the same, the backscattered sound pressure amplitude varies obviously with dimensionless wavenumber ka. The backscattered amplitude (scattering angle 180°) reaches the maximum when dimensionless wavenumber ka is 0.5. According to the definition of dimensionless wavenumber (Eq. (8)), dimensionless wavenumber ka is proportional to the product of ultrasonic frequency and particle radius when the continuous phase is known (i.e. when c is determined), to be precise:

$$ka = (2\pi/c)fr = (2\cdot 3.14/339.9)fr \approx 0.018fr. \qquad (19)$$

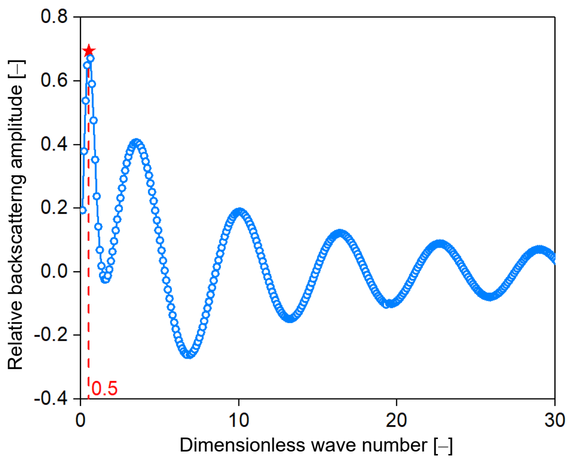

Fig. 10. The relation curve of relative backscattering amplitude versus dimensionless wavenumber ka.

The backscattering amplitude reaches the maximum when dimensionless wavenumber ka is 0.5, in other words, when the product of ultrasonic frequency and particle radius is 27.78 Hz · m (Eq. (20)), the backscattering intensity is the largest:

$$fr = ka/0.018 = 0.5/0.018 \approx 27.78 \text{ Hz}\cdot\text{m}. \qquad (20)$$

That is to say, the closer to 27.78 Hz · m the product of ultrasonic frequency and particle radius is, the larger the amplitude of backscattering will be. Take the case with the frequency of 30 kHz and the radius of 1 mm as an example, the product of ultrasonic frequency and particle radius:

$$fr = 30000 \cdot 0.001 = 30 \text{ Hz} \cdot \text{m}. \tag{21}$$

Compared with the case of the same frequency and other radii, the product of the two is the closest to 27.78 Hz · m (the others are 6 Hz · m, 9 Hz · m, 12 Hz · m, and 18 Hz · m), so the backscattered equivalent voltage reaches the maximum at this time. This is why the higher the frequency in the COMSOL simulation, the smaller the particle radius corresponding to the maximum backscattering amplitude. Thus, the results of COMSOL simulation are verified by the Faran model.

3.3.3. The effect of concentration on backscattering

It can be seen from Fig. 9 that the equivalent voltage of backscattering reaches its maximum at 100 kHz and 0.3 mm when the ultrasonic frequency changes from 30 to 150 kHz and particle radius from 0.2 to 1.0 mm. Therefore, 100 kHz and 0.3 mm are selected respectively as the simulation conditions to explore the effect of the concentration of backscattering intensity.

In the simulation, the mass concentration was 10%, 30%, 50%, and 70%, respectively. To realize the change of mass concentration, the number of particles needed to be changed, and the relationship between the number of particles n and the mass concentration γ_m is shown as follows:

$$\gamma_m = \frac{nS_p}{S_s}\rho_p = \frac{n\pi r^2}{\pi R^2}\rho_p = 2250n\left(\frac{0.3}{150}\right)^2 = 0.009n, \tag{22}$$

where S_p and S_s stand for the cross-sectional area of individual particles and the pipe respectively, ρ_p is the density of granular materials, r and R refer to the radius of individual particle and the pipe.

According to the calculation, when the mass concentration is 10%, 30%, 50%, and 70%, the number of particles to be arranged in the simulation is 12, 34, 56, and 78, respectively. Other conditions for simulation are the same as described before, and the final variation of backscattering intensity with the concentration is shown in Fig. 11. It can be summarized that the backscattering equivalent voltage does not increase with the increase in mass concentration, but maximizes at a concentration of 30%.

3.3.4. Verification of the effect of concentration on backscattering

Similarly, the results of COMSOL simulation are verified with the backscattering model modified by PERCUS and YEVICK (1958). Based on the theory

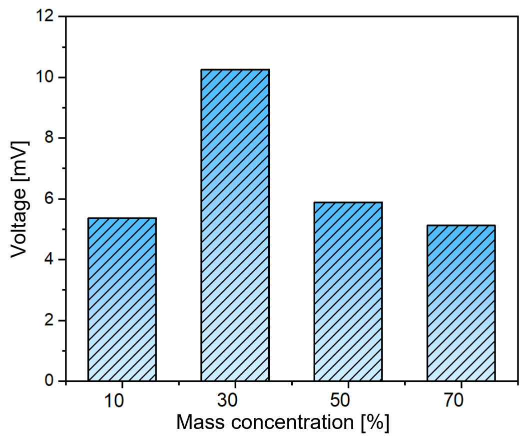

Fig. 11. Histogram of backscattered equivalent voltage varying with mass concentration.

of Sec. 2, when there are more particles in the two-phase flow, the total backscattering sound pressure is proportional to the product of concentration and filling factor, so the change of total sound pressure with concentration can be reflected by representing the product of the two with the change of concentration. Figure 12 shows the change of backscattering intensity with concentration obtained by the modified model. It can be seen from the figure that when the concentration is 32.4%, the product of concentration and packing factor reaches the maximum, that is, the scattering reaches the strongest. The result is consistent with the results obtained by COMSOL simulation. Therefore, the accuracy of simulation can be proved.

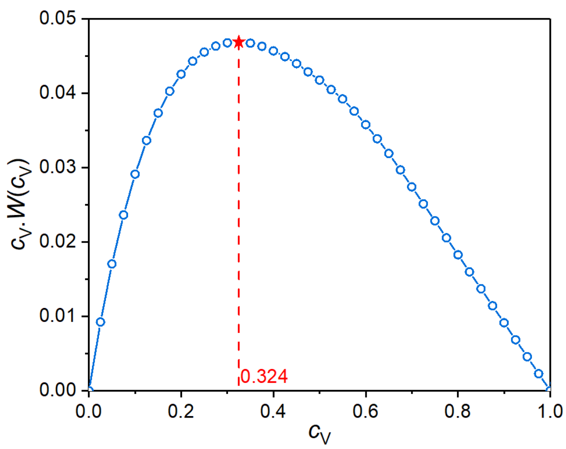

Fig. 12. The relation curve of the product of concentration and packing factor versus concentration.

4. Discussion

4.1. The effect of particle radius on backscattering at different frequencies

Based on the simulation results shown in Fig. 9, the backscattering intensities with the ultrasonic frequency between 75 kHz and 150 kHz are much larger than that when the frequency is smaller (30 kHz, 50 kHz). For this result the explanation is that the larger the ultrasonic frequency is, the smaller the wavelength of the corresponding sound wave will be, and the smaller the ratio of wavelength to particle radius will be, making the scattering effect more obvious, thus the backscattering amplitude gets larger (Rank, McKelvey, 1949; Dukhin, Goetz, 1996; 2001).

Besides, when the frequency changes from 30 kHz to 150 kHz, the backscattered equivalent voltage does not become larger and larger, but reaches its maximum value at 100 kHz, and the differences among the scattered equivalent voltage from 0.3 to 0.6 mm are significant at 100 kHz. The reason is that, although the scattering effect is more apparent with the increase of frequency, there is also the attenuation of sound in the air, and the degree of attenuation is directly proportional to the square of the frequency. With the increase in frequency, the attenuation gets more obvious and the backscattering amplitude is larger. When the influence of attenuation is greater than that of increased backscattering, the intensity will gradually decrease instead (Awad *et al.*, 2012; Challis *et al.*, 2005). Therefore, the comprehensive analysis must be carried out in the practical measurement to select a more appropriate ultrasonic frequency.

4.2. The effect of particle concentration on backscattering at different frequencies

As we can see from Figs 11 and 12, the backscattering equivalent voltage does not get stronger with the increase of the concentration, but presents an optimal value at the concentration of 30%. When the concentration is low, the total backscattering intensity can be regarded as the sum of the backscattering intensity of each particle (Flax *et al.*, 1978). As the concentration increases, the number of particles increases, leading to the increase of backscattering intensity. However, when the concentration increases to a certain degree, the interaction between particles becomes significant, for example, the backward scattered waves of one particle may be blocked by another, and the collision between particles changes the propagation direction of the sound waves. This leads to the phenomenon, that the total strength of backscattering is no longer the sum of the backscattering of many single particles, and even decreases with the increase in the concentration (Pessôa, Neves, 2020; McClements, 1991; Lax, 1951).

5. Conclusions

The finite element software COMSOL was used to simulate the application of the ultrasonic backscattering method in the gas-solid two-phase flow. The results show that the intensity of backscattering is related to the particle radius, concentration and ultrasonic frequency. Given the gas-solid two-phase flow in this paper, when the dimensionless wavenumber ka is 0.5, the backscattering amplitude is the largest, that is, the product of ultrasonic frequency and particle radius is about 27.78 $\mathrm{Hz \cdot m}$. When the concentration is small, the particles can be considered to be no interaction and the total intensity of backscattering is the sum of all individual particles. Therefore, the higher the concentration, the stronger the backscattering intensity. However, the interactions between particles are no longer negligible when the concentration reaches a certain level (up to about 30%). At this time, part of the backscattered sound waves will be blocked and the propagation direction changes, as a result, the increase of the concentration will have an adverse effect on the backscattering intensity, making the backscattered intensity decrease. In conclusion, this work can provide the theoretical basis and guidance for the selection of ultrasonic frequency and concentration in practical applications, and a novel solution for the convenient measurement in the gas-solid two-phase flow field.

Acknowledgments

This work was supported by the National Nature Science Foundation of China (No. 51976188) and the National Key R&D Program of China (No. 2019YFC 1907000).

Declaration of interests

The authors declare that they have no known competing financial interests or personal relationships that could have appeared to influence the work reported in this paper.

References

1. Anderson V.C. (1950), Sound scattering from a fluid sphere, *The Journal of the Acoustical Society of America*, **22**(4): 426–431, doi: 10.1121/1.1906621.

2. Awad T.S., Moharram H.A., Shaltout O.E., Asker D., Youssef M.M. (2012), Applications of ultrasound in analysis, processing and quality control of food: A review, *Food Research International*, **48**(2): 410–427, doi: 10.1016/j.foodres.2012.05.004.

3. Boonkhao B., Wang X.Z. (2012), Ultrasonic attenuation spectroscopy for multivariate statistical process control in nanomaterial processing, *Particuology*, **10**(2): 196–202, doi: 10.1016/j.partic.2011.11.009.

4. Cai X., Li J., Ouyang X., Zhao Z., Su M. (2005), In-line measurement of pneumatically conveyed particles by a light transmission fluctuation method, *Flow Mea-*

surement and Instrumentation, **16**(5): 315–320, doi: 10.1016/j.flowmeasinst.2005.03.011.

5. Challis R.E., Povey M., Mather M.L., Holmes A.K. (2005), Ultrasound techniques for characterizing colloidal dispersions, *Reports on Progress in Physics*, **68**(7): 1541–1637, doi: 10.1088/0034-4885/68/7/R01.

6. Chen H. *et al.* (2020), Study on backscattering characteristics of pulsed laser fuze in smoke [in Chinese], *Infrared and Laser Engineering*, **49**(4): 403005–403005, doi: 10.3788/irla202049.0403005.

7. Dong T., Norisuye T., Nakanishi H., Tran-Cong-Miyata Q. (2020), Particle size distribution analysis of oil-in-water emulsions using static and dynamic ultrasound scattering techniques, *Ultrasonics*, **108**: 106–117, doi: 10.1016/j.ultras.2020.106117.

8. Dukhin A.S., Goetz P.J. (1996), Acoustic spectroscopy for concentrated polydisperse colloids with high density contrast, *American Chemical Society*, **12**(21): 4987–4997, doi: 10.1021/la951085y.

9. Dukhin A.S., Goetz P.J. (2001), New developments in acoustic and electroacoustic spectroscopy for characterizing concentrated dispersions, *Colloids and Surfaces A: Physicochemical and Engineering Aspects*, **192**: 267–306, doi: 10.1016/S0927-7757(01)00730-0.

10. Dukhin A.S., Goetz P.J., Wines T.H., Somasundaran P. (2000), Acoustic and electroacoustic spectroscopy, *Colloids and Surfaces A: Physicochemical and Engineering Aspects*, **173**(1–3): 127–158, doi: 10.1016/S0927-7757(00)00593-8.

11. Elvira L., Vera P., Cañadas F.J., Shukla S.K., Montero F. (2016), Concentration measurement of yeast suspensions using high frequency ultrasound backscattering, *Ultrasonics*, **64**: 151–161, doi: 10.1016/j.ultras.2015.08.009.

12. Epstein P.S., Carhart R.R. (1953), The absorption of sound in suspensions and emulsion. I. Water fog in air, *The Journal of the Acoustical Society of America*, **25**(3): 553–565, doi: 10.1121/1.1907107.

13. Faran Jr. J.J. (1951), Sound scattering by solid cylinders and spheres, *The Journal of the Acoustical Society of America*, **23**(4): 405–418, doi: 10.1121/1.1906780.

14. Flax L., Dragonette L.R., Überall H. (1978), Theory of elastic resonance excitation by sound scattering, *The Journal of the Acoustoical Society of America*, **63**(3): 723–731, doi: 10.1121/1.381780.

15. Furlan J.M., Mundla V., Kadambi J., Hoyt N., Visintainer R., Addie G. (2012), Development of A-scan ultrasound technique for measuring local particle concentration in slurry flows, *Powder Technology*, **215–216**: 174–184, doi: 10.1016/j.powtec.2011.09.044.

16. Gu J., Su M., Cai X. (2018), In-line measurement of pulverized coal concentration and size in pneumatic pipelines using dual-frequency ultrasound, *Applied Acoustics*, **138**: 163–170, doi: 10.1016/j.apacoust.2018.03.034.

17. Han Y.F., Zhao A., Zhang H.X., Ren Y.Y., Liu W.X., Jin N.D. (2016), Differential pressure method for measuring water holdup of oil–water two-phase flow with low velocity and high water-cut, *Experimental Thermal and Fluid Science*, **72**: 197–209, doi: 10.1016/j.expthermflusci.2015.11.008.

18. Hwang C., Chen M.-Y. (2007), Analysis and optimal control of time-varying linear systems via shifted Legendre polynomials, *International Journal of Control*, **41**(5): 1317–1330, doi: 10.1080/0020718508961200.

19. Jia H., Li X., Meng X. (2017), Rigid and elastic acoustic scattering signal separation for underwater target, *The Journal of the Acoustical Society of America*, **142**(2): 653, doi: 10.1121/1.4996127.

20. Jing J., Li Z., Zhu Q., Chen Z., Ren F. (2011), Influence of primary air ratio on flow and combustion characteristics and NO_x emissions of a new swirl coal burner, *Energy*, **36**(2): 1206–1213, doi: 10.1016/j.energy.2010.11.025.

21. Khushrushahi S., Zahn M. (2011), Ultrasound velocimetry of ferrofluid spin-up flow measurements using a spherical coil assembly to impose a uniform rotating magnetic field, *Journal of Magnetism and Magnetic Materials*, **323**(10): 1302–1308, doi: 10.1016/j.jmmm.2010.11.035.

22. Lax M. (1951), Multiple scattering of waves, *Reviews of Modern Physics*, **23**(4): 287–310, doi: 10.1103/RevModPhys.23.287.

23. Louisnard O. (2012), A simple model of ultrasound propagation in a cavitating liquid, Part I: Theory, nonlinear attenuation and traveling wave generation, *Ultrasonics Sonochemistry*, **19**(1): 56–65, doi: 10.1016/j.ultsonch.2011.06.007.

24. Ma Y. *et al.* (2021), Influence of probe geometry on the characteristics of optical fiber gas-liquid two-phase flow measurement signals, *Applied Optics*, **60**(6): 1660–1666, doi: 10.1364/AO.414041.

25. Mathieu J., Schweitzer P. (2004), Measurement of liquid density by ultrasound backscattering analysis, *Measurement Science and Technology*, **15**(5): 869–876, doi: 10.1088/0957-0233/15/5/012.

26. McClements D.J. (1991), Ultrasonic characterisation of emulsions and suspensions, *Advances in Colloid and Interface Science*, **37**(1–2): 33–72, doi: 10.1016/0001-8686(91)80038-L.

27. Meng Z., Huang Z., Wang B., Ji H., Li H., Yan Y. (2010), Air–water two-phase flow measurement using a Venturi meter and an electrical resistance tomography sensor, *Flow Measurement and Instrumentation*, **21**(3): 268–276, doi: 10.1016/j.flowmeasinst.2010.02.006.

28. Percus J.K., Yevick G.J. (1958), Analysis of classical statistical mechanics by means of collective coor-

dinates, *Physical Review*, **110**(1): 1–13, doi: 10.1103/PhysRev.110.1.

29. Pessôa M.A.S., Neves A.A.R. (2020), Acoustic scattering and forces on an arbitrarily sized fluid sphere by a general acoustic field, *Journal of Sound and Vibration*, **479**: 115373, doi: 10.1016/j.jsv.2020.115373.

30. Rank D.H., McKelvey J.P. (1949), A study of the mechanism of modified Rayleigh scattering, *Journal of the Optical Society of America B*, **39**(9): 762–765, doi: 10.1364/josa.39.000762.

31. Sakamoto A., Saito T. (2012), Computational analysis of responses of a wedge-shaped-tip optical fiber probe in bubble measurement, *Review of Scientific Instruments*, **83**(7): 075107, doi: 10.1063/1.4732819.

32. Shaffer F.D., Bajura R.A. (1990), Analysis of Venturi performance for gas-particle flows, *Journal of Fluids Engineering*, **112**(1): 121–127, doi: 10.1115/1.2909359.

33. Tian C., Su M., Chen X., Cai X. (2013), An investigation on ultrasonic process tomography system for particle two-phase flow measurement [in Chinese], *Journal of NanJing University (Natural Sciences)*, **49**(1): 20–26, doi: 10.13232/j.cnki.jnju.2013.01.017.

34. Tsuji K., Norisuye T., Nakanishi H., Tran-Cong-Miyata Q. (2019), Simultaneous measurements of ultrasound attenuation, phase velocity, thickness, and density spectra of polymeric sheets, *Ultrasonics*, **99**: 105974, doi: 10.1016/j.ultras.2019.105974.

35. Twerskyt V. (1975), Transparency of pair-correlated, random distributions of small scatterers, with applications to the cornea, *Journal of the Optical Society of America*, **65**(5): 524–530, doi: 10.1364/JOSA.65.000524.

36. Wang Y. *et al.* (2016), The simulation analysis of effect with particles in different sizes on ultrasonic measurement of gas-solid two phase flow, [in:] *Proceedings of 2016 International Conference on Wireless Communication and Network Engineering* (WCNE 2016), pp. 307–310.

37. Wang Y., Lyu X., Li W., Yao G., Bai J., Bao A. (2018), Investigation on measurement of size and concentration of solid phase particles in gas-solid two phase flow, *Chinese Journal of Electronics*, **27**(2): 381–385, doi: 10.1049/cje.2017.12.005.

38. Wang Y., Yao G., Zhang Y., Liu M., Ge P. (2017), Ultrasonic radial simulation research of solid particle distribution of segregation flow in gas-solid two phase flow, [in:] *Proceedings of the 2017 2nd International Conference on Automation, Mechanical and Electrical Engineering (AMEE 2017), Advances in Engineering*, **87**: 61–64, doi: 10.2991/amee-17.2017.12.

39. Weser R., Woeckel S., Wessely B., Steinmann U., Babick F., Stintz M. (2014), Ultrasonic backscattering method for in-situ characterisation of concentrated dispersions, *Powder Technology*, **268**: 177–190, doi: 10.1016/j.powtec.2014.08.026.

40. Weser R., Wöckel S., Wessely B., Hempel U. (2013), Particle characterisation in highly concentrated dispersions using ultrasonic backscattering method, *Ultrasonics*, **53**(3): 706–716, doi: 10.1016/j.ultras.2012.10.013.

41. Yao J., Takei M. (2017), Application of process tomography to multiphase flow measurement in industrial and biomedical fields: a review, *IEEE Sensors Journal*, **17**(24): 8196–8205, doi: 10.1109/jsen.2017.2682929.